Supporting Information

Wearable Temperature Sensors with Enhanced Sensitivity by Engineering Microcrack Morphology in PEDOT:PSS-PDMS Sensors

Yuyan Yu[1], Shuhua Peng[1], Philippe Blanloeuil[1], Shuying Wu[2, 1]*, and Chun H. Wang[1]*

[1]School of Mechanical and Manufacturing Engineering, University of New South Wales, Sydney, NSW 2052, Australia

[2]School of Engineering, Macquarie University, Sydney NSW 2109, Australia

*Correspondence author: chun.h.wang@unsw.edu.au; shuying.wu@mq.edu.au.

S1 Crack Parameters, Temperature Sensitivities and Electrical Properties of Sensors

Table S1 summarised the crack parameters and temperature sensing properties of PEDOT:PSS/PDMS sensors from different fabrication processes.

Table S1. Crack parameters and temperature sensing properties of PEDOT:PSS/PDMS sensors via various production conditions.

Substrates	**Acid treat time** (min)	**Pre-stretching stain** (%)	**Average crack length** (μm)	**Crack density** (mm^{-1})	**TCR** ($^oC^{-1}$)	**Linearity**
Smooth	0	0	0.00	0.00	0.00098	$R^2 = 0.999$
Smooth	0	20	0.00	0.00	0.0010	$R^2 = 0.911$
Smooth	0	40	1650.33 ± 240.55	3.63 ± 0.08	0.0080	$R^2 = 0.966$
Smooth	0	80	2590.39 ± 233.14	8.94 ± 0.20	-	-
P320	0	0	0.00	0.00	0.00096	$R^2 = 0.997$
P320	0	20	0.00	0.00	0.0013	$R^2 = 0.996$
P320	0	40	138.91 ± 11.53	5.67 ± 0.02	0.0031	$R^2 = 0.965$
P320	0	80	248.33 ± 24.77	16.55 ± 0.58	0.0039	$R^2 = 0.995$
P800	0	0	0.00	0.00	0.0011	$R^2 = 0.997$
P800	0	20	0.00	0.00	0.0012	$R^2 = 0.997$
P800	0	40	120.00 ± 4.11	10.08 ± 0.48	0.0041	$R^2 = 0.997$
P800	0	80	247.54 ± 23.43	20.53 ± 0.41	0.0043	$R^2 = 0.998$
P800	90	80	197.61 ± 25.12	20.84 ± 0.37	0.0098	$R^2 = 0.997$
P800	180	80	185.25 ± 15.47	22.84 ± 0.27	0.0420	$R^2 = 0.998$
P800	270	80	299.60 ± 48.14	15.57 ± 0.75	0.0210	$R^2 = 0.989$
P800	360	80	372.19 ± 28.86	11.74 ± 2.88	0.0180	$R^2 = 0.998$
P800	180	0	0.00	0.00	0.00084	$R^2 = 0.993$
P800	180	20	75.14 ± 2.24	12.06 ± 0.66	0.0040	$R^2 = 0.999$
P800	180	40	89.51 ± 3.74	19.32 ± 0.14	0.0065	$R^2 = 0.998$
P800	180	60	161.34 ± 24.81	20.21 ± 0.78	0.0206	$R^2 = 0.996$

Table S2 summarised the *initial* resistance values of PEDOT: PSS-PDMS sensors made form flat, and rough PDMS substrates ***(*$\mathbf{R_0}$*)***, as well as the resistance after pre-stretching ($\mathbf{R_{pre\text{-}tretching}}$) and acid treatment ($\mathbf{R_{acid}}$).

Table S2 Resistance values of Sensors as prepared on various substrates, after acid treatment, and after pre-stretching.

Substrates	**Acid treat time** (min)	**Pre-stretching stain** (%)	$\mathbf{R_0}$ (Ω)	$\mathbf{R_{acid}}$ (Ω)	$\mathbf{R_{pre\text{-}stretching}}$ (Ω)
Smooth	0	0	127.8	-	-
Smooth	0	20	138.6	-	538.0
Smooth	0	40	119.3	-	707.2
Smooth	0	80	149.5	-	3827.56
P320	0	0	297.2	-	-
P320	0	20	265.3	-	283.5
P320	0	40	278.2	-	356.8
P320	0	80	234.5	-	1156.3
P800	0	0	219.0	-	-
P800	0	20	221.5	-	231.8
P800	0	40	205.7	-	294.8
P800	0	80	223.2	-	2517.9
P800	90	80	224.5	192.3	231.8
P800	180	80	216.5	159.3	17885.3
P800	270	80	263.7	162.5	0.0210
P800	360	80	302.5	143.6	0.0180
P800	180	0	216.5	159.3	-
P800	180	20	216.5	159.3	1618.2
P800	180	40	216.5	159.3	3434.6
P800	180	60	216.5	159.3	16834.5

S2. Temperature Sensing Performance Comparison

Table S3 compared temperature sensing performance of the developed PEDOT: PSS/PDMS sensor and other PEDOT: PSS based temperature sensors from literature. Among all reported sensors, our PEDOT: PSS/PDMS sensor stands out with the highest temperature sensitivity at 0.0420 $^{o}C^{-1}$ and excellent linearity at 0.998.

Table S3 Comparison of temperature sensing performance on sensors based on PEDOT: PSS composites.

Sensors	**TCR** ($^{o}C^{-1}$)	**Sensing Range**	**Linearity**	**Reference**
PEDOT coated on PI fibre	-0.0046	15-45	linear	[1]
PNIPAM/PEDOT:PSS/CNT	-0.026	25-40	Linear, R^2= 0.98	[2]
PEDOT coted on cotton thread	- 0.0048	-50-80	Linear, 99.8%	[3]
PEDOT printed on PP	-0.03	-10-20	Nonliner	[4]
PEDOT coted on glass	-0.0041	30-170	Nonlinear	[5]
PEDOT coated on cotton textile	-0.0036	30-150	Nonlinear	[5]
PEDOT coated on Kapton film	-0.0068	30-150	Nonlinear	[5]
PEDOT	-0.0086	20-80	Nonlinear	[6]
PEDOT/graphene	-0.006	35–45	Linear	[7]
PEDOT: PSS/PDMS film	**0.0420**	**30-55**	**Linear, R^2= 0.998**	**This work**

Table S4 compared temperature sensing performance of industrial thermometers and the developed PEDOT: PSS/PDMS sensor.

Table S4 Comparison of performance of body temperature measuring methods.

Sensors	**Sensing Range** (ºC)	**Resolution** ($^{o}C^{-1}$)	**Wearability**	**Continuous Monitoring**	**Reference**
Mercury Thermometer	30-55	0.1	Not wearable	No	[8]
Digital Thermometer	32 - 41.9	0.1	Not wearable	No	[9]
Infrared forehead thermometer	10 - 40	0.1	Not wearable	No	[10]
Liquid Crystal Forehead Temperature Strips	-30 - 59	1	Wearable	No	[11]
PEDOT: PSS/PDMS film	**30-55**	**0.1**	**Wearable**	**Yes**	**This work**

S3. Properties of Sandpaper Templates

Table S5 summarized the surface roughness parameters of P320 and P800 sandpapers.

Table S5. Roughness parameters of sandpapers used in this work.

Sandpapers	Ra	Rz	Rv	Rp	Rq	Rsk	Rku
P320	17.92	325.5	138.1	187.3	24.6	0.2388	5.008
P800	6.273	119.4	45.35	74.05	8.492	0.6921	5.516

The rough PDMS substrates are made by casting uncured liquid PDMS mixture to the surface of commercial sandpapers to copy the morphology of sandpapers, and the SEM images of the two types of sandpapers and corresponding rough PDMS substrates are shown in the Figure S1.

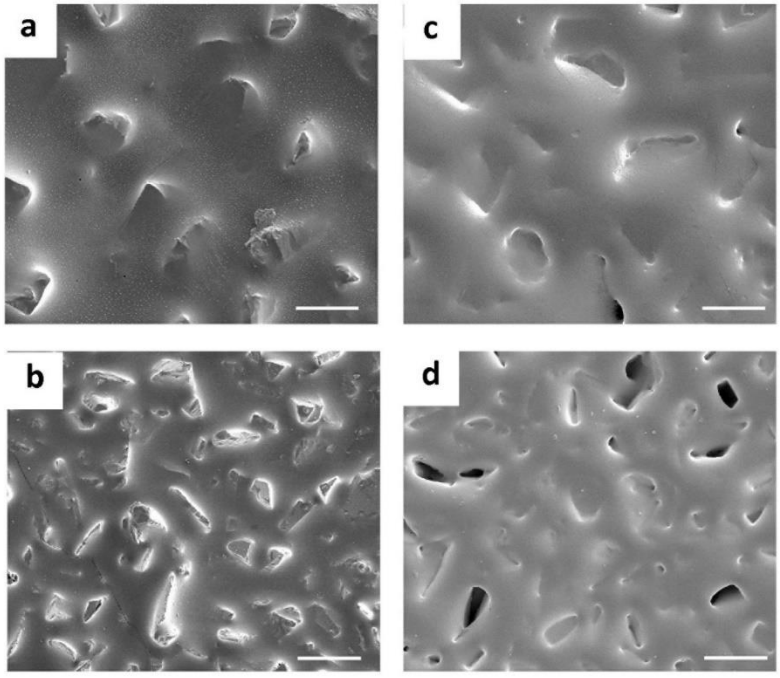

Figure S1. SEM images of commercial sandpapers P320 (a) and P800 (b) and the corresponding rough PDMS substrates made from sandpapers P320 (c) and P800 (d). Scale bar: 50 μm.

S4. Crack morphology at 20% Strain

Typical optical images of PEDOT:PSS/PDMS sensors fabricated with various substrates at pre-stretching strain of 20% were shown in Figure S2 Typical optical images of PEDOT:PSS/PDMS sensors fabricated with various substrates, all taken at 20% strain.

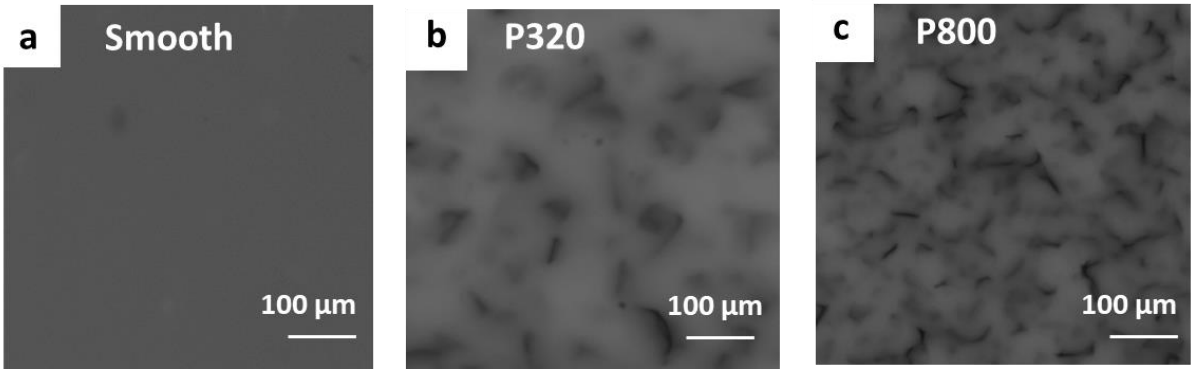

Figure S2 Typical optical images of PEDOT:PSS/PDMS sensors fabricated with various substrates, all taken at 20% strain.

S5. Image Processing Method

A multi-step image processing was performed in view of extracting the cracked area from the optical images, as shown in Figure S3a-b. First, the colour image was converted into a greyscale image, where the intensity of the image was adjusted to improve the contrast between the cracks and the background, as shown in Figure S3a. Second, the crack-like structures were enhanced using multi-scale Hessian filtering techniques developed for angiographic images processing[12, 13], as shown in Figure S3b. The resulting image was then converted into a binary image, as shown in Figure S3c, where blobs having an aspect ratio lower than 5 were excluded, i.e. only the elongated, crack-like structures were retained. The final image can then be compared with the initial colored images, demonstrating that the cracks are correctly identified, as shown in Figure S3d, where the previous image processing steps were applied onto the images obtained for PEDOT: PSS/PDMS samples under 80% strain. Afterwards, the crack information, such as the average crack length (l_a) and average crack number (N) can be extracted. The N is the average number of cracks at each line in the direction vertiacal to the crack oritetion. The crack density (D) is defined as the average gaps between two cracks in the direction vertical to the crack propagation path and is given by:

$$D = \frac{L}{N + 1} \tag{S1}$$

Where N is the average crack number, and L is the length of the image.

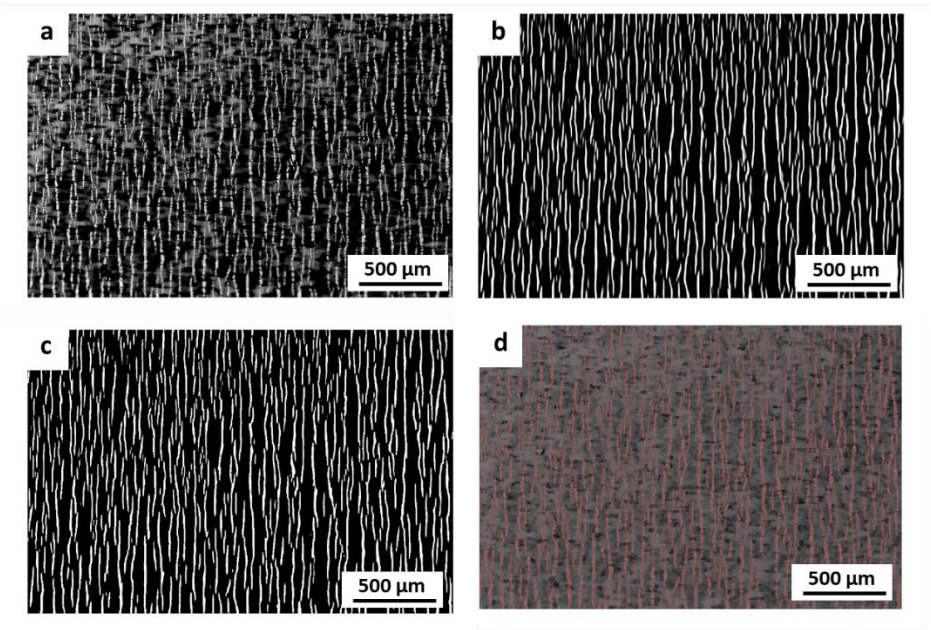

Figure S3. Image processing steps applied onto a 4248-by-2832 pixel area of an image obtained under 80% strain for the PEDOT: PSS/PDMS sample, after (a) greyscale conversion and scale adjustment, (b) crack-like structure enhancement using multi-scale Hessian filtering [1,2], (c) binary image conversion and aspect ratio filtering. (d) Identified cracks superimposed on original images.

S6. Peeling-off Test

The adhesion of PEDOT: PSS films on PDMS substrates was evaluated through a peeling test by 3M adhesive tape.

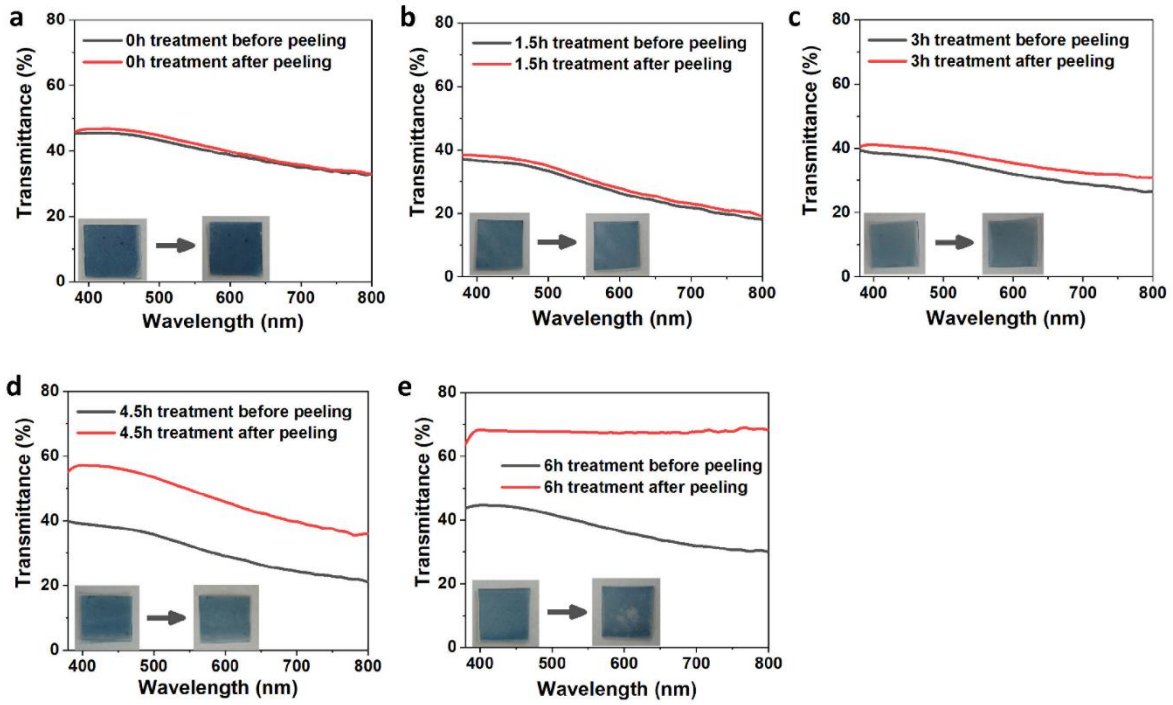

Figure S*4* showed the UV–Vis transmittance spectra of films subjected to sulfuric acid treatment before and after peeling. The digital photos of films before and after peeling were also displayed in the corresponding graphs. Without acid treatment

(

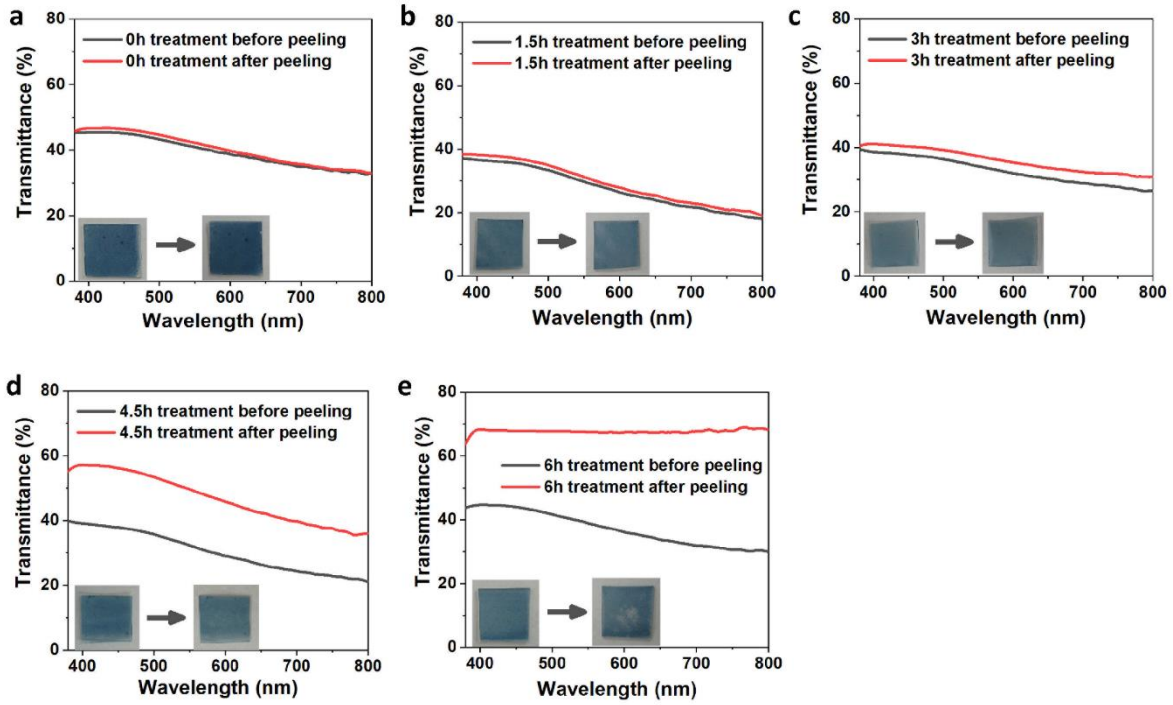

Figure S4a), both the transmittance spectra and the film remains unchanged after peeling, indicating good adhesion of PEDOT: PSS layer to PDMS substrate. When the films were subjected to 1.5 h and 3 h acid treatment

(

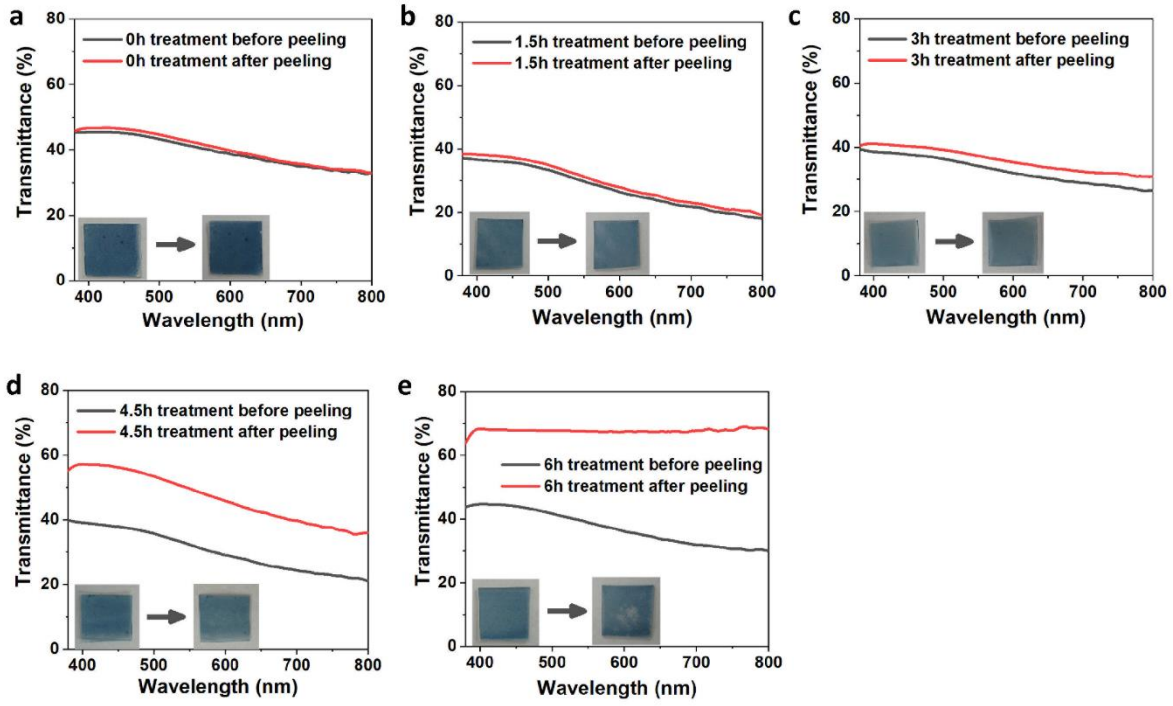

Figure S4b-c), although no obvious detachment visible form the digital photos, the transmittance spectra slightly moved upwards after peeling, which indicated that the adhesion

of PEDOT:PSS film is slightly weakened. However, once the acid treatment time increased to over 4.5 h (

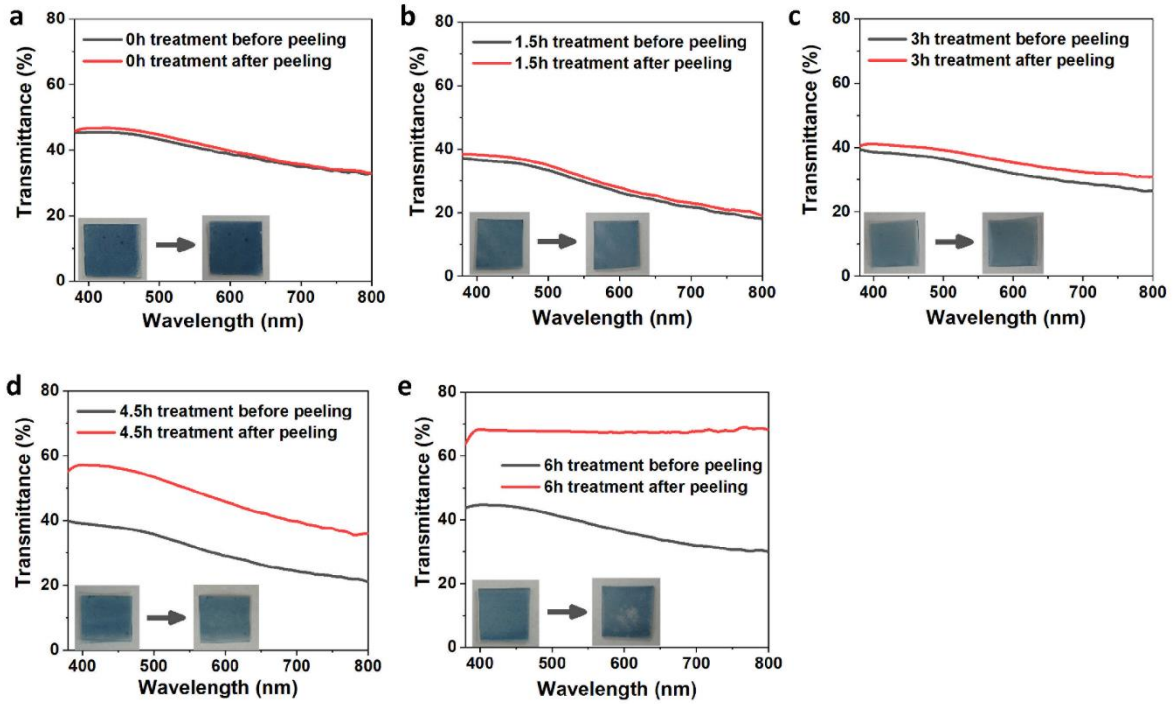

Figure S4d-e), serous detachment of PEDOT: PSS film from the substrate can be observed due to the poor adhesion, as is implied by the increased transmittance spectra.

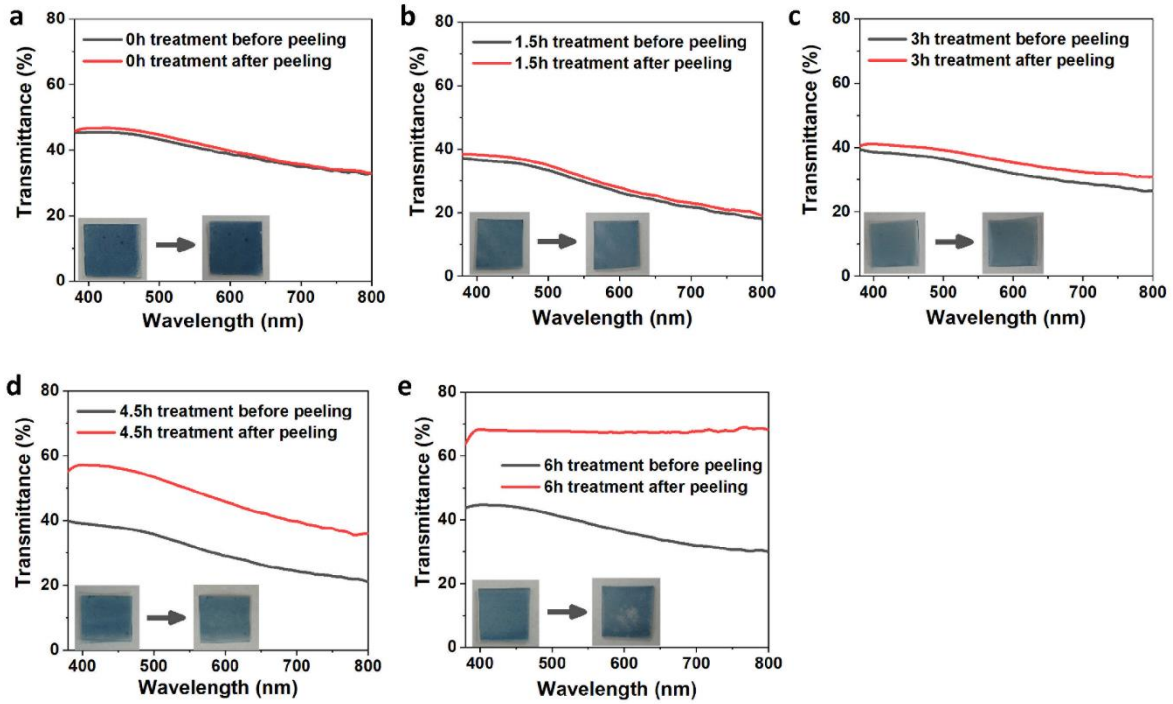

Figure S4. UV–Vis transmittance spectra of PEDOT: PSS/PDMS films treated by 1 M sulfuric acid solution for a various times before and after peeling by the tape. The insets are the digital images of the corresponding films.

S7. Standard Variation of Optimized Sensor

The TCR of there individually made sensors with this optimized process parameters were tested, and the result shows a small statistic variation of 0.0059 $°C^{-1}$.

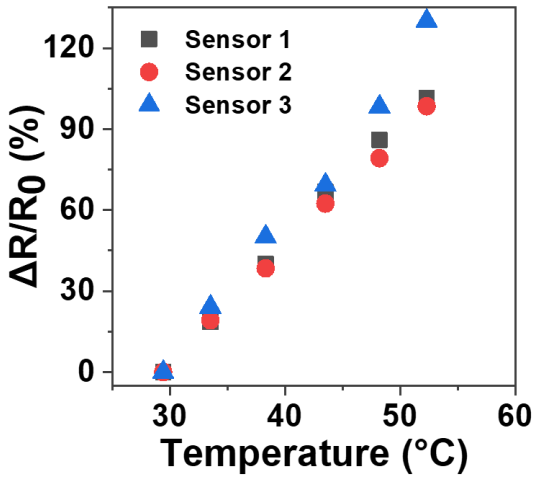

Sensors	**TCR** ($°C^{-1}$)
Sensor 1	0.045
Sensor 2	0.054
Sensor 3	0.043
Standard variation	0.0059
Coefficient of variation	12.5%

Figure S5 Relative resistance changes and TCR values of three individually made PEDOT PDMS sensors (rough substrate, 180 min acid treatment, 80% pre-stretching strain) in the temperature range from 30 to 55 °C.

S8. Piezoresistivity of the Optimized Sensor

Figure S6 presents the effect of mechanical strain under isothermal condition (constant temperature) on the Piezoresistivity of the optimized sensor.

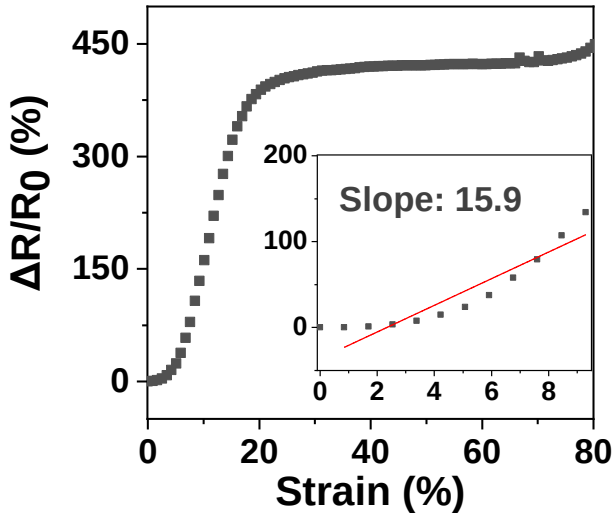

Figure S6 Relative resistance changes vs. strain curve of PEDOT:PSS-PDMS sensor with the optimized TCR.

S9. **Detection Limit**

The temperature change corresponding to a measured resistance change can be calculated using the following relationship

$$\Delta T = \frac{1}{TCR}\frac{\Delta R}{R_0} \quad \text{(S2)}$$

The accuracy of the PEDOT:PSS-PDMS sensors in detecting small temperature change is an essential consideration for practical applications. The smallest temperature change that can be detected depends on the signal to noise ratio (SNR= $(\mu/\sigma)^2$) of the sensor. Here the signal, μ, is defined as the average value of the relative resistance change, i.e., $\mu = \text{average}(\frac{\Delta R(t)}{R_0})$, and σ is the standard deviation of the noise, i.e., $\sigma = (\frac{\Delta R(t)}{R_0} - \mu)$.

In the present case, there are two sources for the measurement noise: (a) the Johnson noise of sensors, generated by the thermal agitation of the charge carriers and (b) the intrinsic system noise of the measurement instrument.

In a narrow band of frequencies, Δf, the contribution to the mean-squared noise voltage $\overline{V_n^2}$ from the thermal agitation is:

$$\overline{V_n^2} = 4Rk_BT\Delta f \quad \text{(S3)}$$

where R is the resistance in ohms and T is the temperature in degrees Kelvin for the resistor, k_B is the Boltzmann constant (1.38×10^{-23} J/K).

This noise voltage is too small to be detected without amplification. We have conducted further experiments using the circuit (Figure S7) with an amplifier (gain at 40 times) to measure the Johnson noise, and the recorded root mean square noises are shown in Table S6. The results show that all the carbon film standard standard resistors (their electronic noise is described by the Johnson–Nyquist noise theory) and our piezoresistive sensors have similar RMS noises, indicating that the recorded noises are dominated by the system noise and the piezoresistive sensors have comparable noise as the carbon film standard resistors. The Johnson noises are still too small to be measured even with the amplifier (Response Plus, EIP series 700) to gain the signal. We can estimate that the RMS noise ($\sqrt{\overline{V_n^2}}$) of sensors (100 Ω to 20 KΩ) according to equation (3). The RMS noise of sensors should be in the range from 0.04 to 8 μVat room

temperature and a 10 kHz bandwidth, which is very small compared to the voltage difference (0.1 to 20V) across the sensors when using a multimeter to test the resistance value. So the Johnson noise of sensors is ignorable compared to the relatively large noise of the measurement instrument.

The total noise associated with a sensor-instrument system can be determined by measuring the electrical resistance using a digital multimeter operating at a given sampling rate. The noise values for two PEDOT:PSS sensors with different TCR values measured at a temperature of 25 °C under different sampling rates are plotted in Figure S8. The noise in these measurements, particularly above 10 Hz, is most likely due to interference from the AC power supply, which is at 50 Hz. It can be seen the sensor with the higher temperature sensitivity is slightly noisier than the sensor with a lower sensitivity, particularly at measurement sampling frequencies below 10 Hz. For both sensors, the noise increases with the sampling rate, as expected.

Taking the detection limit as the signal being 6 dB above the noise floor, which equates to μ being twice the noise σ, the smallest temperature change that can be detected with high probability of detection and low false alarm rate is

$$\Delta T_{limit} = \frac{2}{TCR}\sigma \quad \text{(S4)}$$

The calculated detection limits for the sensors with the higher and the lower TCR values are 0.12 °C and 0.08 °C, respectively.

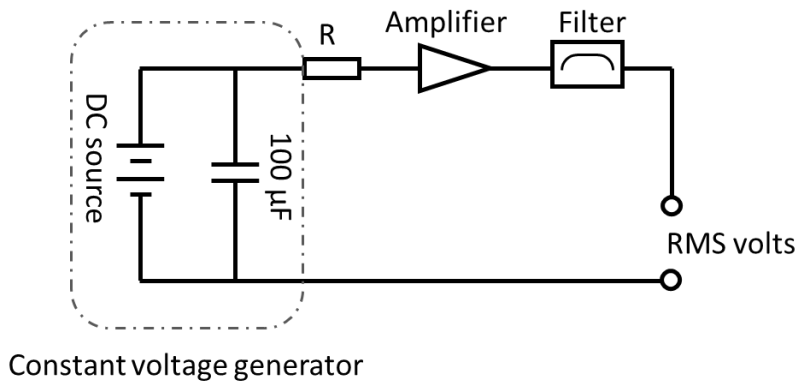

Figure S7 Circuit for testing Johnson noise of sensors.

Table S6 Recorded RMS voltage of carbon film resistors and demonstrated sensors

Sample	Resistance (KΩ)	RMS Voltage of measurement (V)
Carbon film resistor	0.1	6.54314E-05
Carbon film resistor	0.15	6.42704E-05
Carbon film resistor	1	6.52285E-05
Carbon film resistor	2	6.18469E-05
Carbon film resistor	10	6.27482E-05
Carbon film resistor	22	6.66068E-05
Carbon film resistor	100	6.46787E-05
Sensor 1	7.05	6.13107E-05
Sensor 2	0.97	6.27509E-05

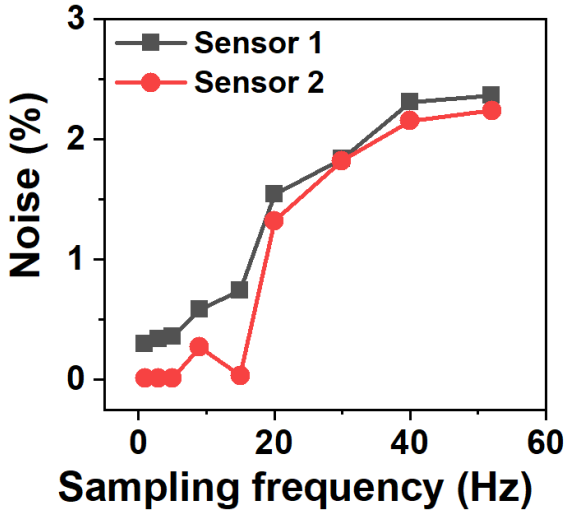

Figure S8 Noise of temperature sensors versus sampling rate with Keysight 34465a digital multimeter.

S10. Linearity Explanation

The electrical resistance, *R*, of a material can increase or decrease with temperature, and the relationship is approximately liner when the temperature does not vary too much from a reference temperature

$$\frac{R}{R_0} = 1 + \alpha\frac{T-T_0}{T_0}, \quad (T - T_0)/T_0 \ll 1.0 \tag{S5}$$

where R_0 is the resistance at a reference temperature T_0 (usually room temperature). For semiconductors, the intrinsic resistance decreases with temperature, and this relationship is often described by an exponential relationship

$$R = R_\infty e^{\alpha/T} \tag{S6}$$

where R_∞ denotes the resistance at infinitely high temperature ($T \to \infty$), $\alpha = E_a/2K$ where E_a is the thermal activation energy, and *K* is the Boltzmann constant. Denoting a reference temperature as T_0, therefore, the formula for relative temperature change can be written as

$$\frac{\Delta R}{R_0} = e^{\frac{\alpha}{T}-\frac{\alpha}{T_0}} - 1 \approx -\frac{\alpha\Delta T}{T_0(T_0+\Delta T)} \approx -\frac{\alpha}{T_0^2}\Delta T \quad , \ \Delta T \ll T_0 \tag{S7}$$

So, the TCR can be well approximated by a linear relationship with temperature within a moderately narrow temperature range ($\Delta T/T_0 \ll 1$).

S11. Cross-sensitivity

The temperature sensors are sensitive to both temperature change and the mechanical stretch. First of all, the sensing performance of the sensors has been characterized at 10% strain and the results are presented in Figure S11, which shows that the temperature performance remains largely the same under constant strain. To avoid the influence of varying mechanical strain due to human movements, structural design methods, such as strain isolation method, can be employed to suppress the external strain effect (*Science* 355.6320 (2017): 59-64.).

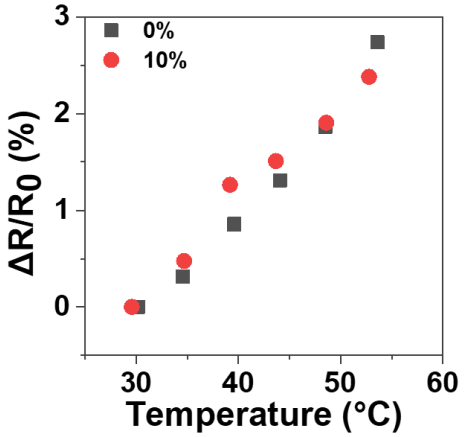

Figure S9 Relative resistance change of sensors at zero-strain and 10% strain in the temperature range from 30 to 55 °C.

References

[1] Daoud, W. A.; Xin, J. H.; Szeto, Y. S., Polyethylenedioxythiophene Coatings for Humidity, Temperature and Strain Sensing Polyamide Fibers. *Sensor Actuat B-Chem* **2005,** *109* (2), 329-333.

[2] Oh, J. H.; Hong, S. Y.; Park, H.; Jin, S. W.; Jeong, Y. R.; Oh, S. Y.; Yun, J.; Lee, H.; Kim, J. W.; Ha, J. S., Fabrication of High-Sensitivity Skin-Attachable Temperature Sensors with Bioinspired Microstructured Adhesive. *Acs Applied Materials & Interfaces* **2018,** *10* (8), 7263-7270.

[3] Lee, J. W.; Han, D. C.; Shin, H. J.; Yeom, S. H.; Ju, B. K.; Lee, W., Pedot:Pss-Based Temperature-Detection Thread for Wearable Devices. *Sensors-Basel* **2018,** *18* (9), 2996.

[4] Maslik, J.; Andersson, H.; Forsberg, V.; Engholm, M.; Zhang, R.; Olin, H., Pedot: Pss Temperature Sensor Ink-Jet Printed on Paper Substrate. *J Instrum* **2018,** *13*, C12010.

[5] Zhang, Y. L.; Cui, Y., Development of Flexible and Wearable Temperature Sensors Based on Pedot:Pss. *Ieee T Electron Dev* **2019,** *66* (7), 3129-3133.

[6] Nitani, M.; Nakayama, K.; Maeda, K.; Omori, M.; Uno, M., Organic Temperature Sensors Based on Conductive Polymers Patterned by a Selective-Wetting Method. *Org Electron* **2019,** *71*, 164-168.

[7] Vuorinen, T.; Niittynen, J.; Kankkunen, T.; Kraft, T. M.; Mantysalo, M., Inkjet-Printed Graphene/Pedot:Pss Temperature Sensors on a Skin-Conformable Polyurethane Substrate. *Sci Rep-Uk* **2016,** *6*, 35289.

[8] Latman, N. S.; Hans, P.; Nicholson, L.; DeLee, S. Z.; Lewis, K.; Shirey, A., Evaluation of Clinical Thermometers for Accuracy and Reliability. *Biomedical instrumentation technology* **2001,** *35* (4), 259-265.

[9] Digital Thermometer for Body Temperature 32-41.9°C Beeper. https://www.seton.net.au/digital-thermometer-for-body-temperature-beeper-a22882.html?source=google_shopping&gclid=Cj0KCQjww_f2BRC-ARIsAP3zarEmpEPg1cMAjVlON_YZznz8PIvg3OILbh6JYYz0JyeKHk7n-YZhfXoaAgO_EALw_wcB.

[10] Infrared Non-Contact Forehead Thermometer. https://www.seton.net.au/infrared-forehead-thermometer.html.

[11] Liquid Crystal Thermometers https://www.hallcrest.com/color-change-basics/liquid-crystal-thermometers.

[12] Jerman, T.; Pernus, F.; Likar, B.; Spiclin, Z., Enhancement of Vascular Structures in 3d and 2d Angiographic Images. *Ieee T Med Imaging* **2016,** *35* (9), 2107-2118.

[13] Jerman, T.; Pernus, F.; Likar, B.; Spiclin, Z., Blob Enhancement and Visualization for Improved Intracranial Aneurysm Detection. *Ieee T Vis Comput Gr* **2016,** *22* (6), 1705-1717.